Supporting Information

Two-Dimensional Pd–C Bonded Organometallic Framework with Dynamic Packing Transformations

[a] Department of Chemistry, Korea Advanced Institute of Science and Technology, 291, Daehak-ro, Yuseong-gu, Daejeon, Republic of Korea, 34141
[b] InnoCORE AI Co-Research & Education for Innovative Drug (AI-CRED) Institute, Korea Advanced Institute of Science and Technology, 291, Daehak-ro, Yuseong-gu, Daejeon, Republic of Korea, 34141
[c] Department of Chemistry Education, Sunchon National University, 255, Jungang-ro, Suncheon-si, Jeollanam-do, Republic of Korea, 57922
[d] Center for Catalytic Hydrocarbon Functionalizations, Institute for Basic Science, 291, Daehak-ro, Yuseong-gu, Daejeon, Republic of Korea, 34141
† These authors contributed equally to this work.

Jong-Yeong Jung,[a,†] Jaewook Kim,[a,b,†] Jintaek Gong,[c] Dongwook Kim,[d] Hee-Seung Lee*[a,b] and Hyunjoon Song*[a,b]

Table of Contents

S1. Experimental Details

Chemicals

All reagents were purchased from commercial sources (Sigma-Aldrich or JUNSEI) and used without further purification. Pd(II) acetate ($Pd(OAc)_2$, 98.0 %, Sigma-Aldrich), terephthalic acid ((H_2bdc), 98.0%, Sigma-Aldrich), and dimethyl sulfoxide (DMSO, 99%, Duksan) were used to synthesize PdOF-1.

Synthesis of PdOF-1

PdOF-1 was synthesized via a solvothermal reaction. 28 mg of $Pd(OAc)_2$ and 42 mg of H_2bdc were dissolved in 6 mL of DMSO. The solution was transferred into a 20 mL vial and heated in an oven at 80 °C for 24 h. After the solution was gradually cooled down to room temperature for 4 h, the yellow product was collected. To maintain PdOF-1 in its pristine PdOF-1(A) phase, the powder must be kept wet with fresh DMSO. For yield determination, PdOF-1(A) was dried under vacuum to remove the residual DMSO adhering to the particle surfaces, resulting in conversion to PdOF-1(B). Based on the chemical composition of PdOF-1(B) determined by SC-XRD ($C_7\ H_{10}\ O_3\ Pd\ S_{1.5}$), the yield of PdOF-1 powders was estimated to be approximately 30%.

Crystal growth for SC-XRD

For SC-XRD, PdOF-1 crystals were synthesized via a solvothermal reaction. 42 mg of $Pd(OAc)_2$ and 90 mg of H_2bdc were dissolved in 15 mL of DMSO. The solution was transferred into a 20 mL vial and heated in an oven at 80 °C for 72 h. After the solution was gradually cooled down to room temperature for 4 h, the yellow crystals were collected.

Preparation of PdOF-1(B) and PdOF-1(C)

PdOF-1(B) and PdOF-1(C) were prepared via thermal treatments of the pristine PdOF-1(A). The pristine PdOF-1(A) transferred into an alumina boat (Samhwa ceramic company) and heated in a tube furnace (Lindberg/Blue M, ThermoFisher Scientific) at 70 and 190 °C for 30 min to prepare PdOF-1(B) and PdOF-1(C), respectively. The temperature rise time was fixed as 20 min. After a gradual cooling down to room temperature for 3 h, the light yellow and dark brown products were collected.

Structure determination of PdOF-1(A) from SC-XRD

The diffraction data of PdOF-1(A) was collected at the Bruker D8 QUEST in Center for Catalytic Hydrocarbon Functionalizations, Institute for Basic Science (IBS). The crystal was sampled on loop holder under stream of N_2 (g) at 173 K. Diffraction patterns were indexed, integrated, and scaled by *APEX4*. Data reduction was carried out with the *xprep* program embedded in *SHELXTL*.[1,2] Structure solution and refinement was performed by direct method on *SHELXT* and *SHELXL*,[3–5] respectively. Detailed crystallographic information is represented in the ***Appendix***.

Structure determination of PdOF-1(B) from SC-XRD

SC-XRD patterns were collected at the 2D-SMC Beamline at Pohang Accelerator Laboratory (Pohang, Korea) using monochromatic synchrotron radiation.[6] The crystal was sampled on loop holder under stream of N_2 (g) at 100K. Diffraction patterns were indexed, integrated, and scaled by *HKL3000sm*.[7] Data reduction was carried out with the *xprep* program embedded in *SHELXTL*.[1,2] Structure solution and refinement was performed by direct method on *SHELXT* and *SHELXL*,[3–5] respectively. *Olex2* GUI system was used for better visualization and functionality during the structure solution and refinement.[8,9] *SQUEEZE* embedded in *Olex2* (solvent mask) was used due to the ambiguous Fourier difference map of the intercalated DMSO solvents.[10] Detailed crystallographic information is represented in the ***Appendix***.

Structure determination of PdOF-1(C) from PXRD

High-resolution PXRD patterns were collected at the 9B-High-Resolution Powder Diffraction (HRPD) beamline at Pohang Accelerator Laboratory (PAL, Pohang-si, Gyeongsangbuk-do, Republic of Korea). The powder was diffracted on monochromatic synchrotron radiation (λ = 1.54600 Å) at room temperature with a step size of 0.005° for a scan time of 1sec per step over the 2θ range 8.5–129.5°. The region after 2θ = 60° was trimmed to exclude silicon holder peaks and patterns with poor signal to ratio. We followed the prevalent structure determination from powder diffraction data (SDPD) procedure described at the previous paper which was published by our group.[11] 20 Peaks with the highest intensity from the PXRD pattern were selected for indexing process by *Crysfire* and a monoclinic unit cell was extracted.[12] The direct space method was used in the structure solution phase with *F.O.X.* program,[13–15] followed by Rietveld refinement with *GSAS/EXPGUI* suite program.[16,17] Although the true space group was $P2_1/a$, the refinement was held at lower symmetry ($P2_1$) to prevent the divergence of the system. Pseudovoigt profile coefficients,[18] asymmetry correction,[19] and microstrain broadening[20] were applied on profile fitting. The Rietveld plot and crystallographic information are represented in the ***Appendix***.

Calculation of Void Space & Porosity in Crystal Structures

Void space was determined using *Mercury* software (probe radius = 1.2 Å, grid spacing = 0.7 Å, *Contact Surface* map),[21] following the reported method.[22] Porosity was calculated by dividing the void space by the total volume of the unit cell. All intercalated DMSO molecules were removed, and excluded hydrogens on PdOF-1(C) were manually added before void space calculation.

PXRD pattern of PdOF-1 with various temperature

Thermal treated PdOF-1 was prepared at various temperature as the same method for the preparation of PdOF-1(B) and PdOF-1(C). The products were collected and transferred to the zero-background XRD holder. Powder X-ray diffraction (PXRD) patterns were analyzed using Smartlab (Rigaku) with a Cu-Ka beam of wavelength 1.5418 Å.

Instruments

Fourier transform-infrared (FT-IR) spectra were analyzed with the Nicolet iS50 (Thermo Fisher Scientific Instrument). Solid-state ^{13}C cross-polarization magic-angle-spinning (CP-MAS) NMR plots were measured by VNMRS 600 Solid system (Varian). X-ray photo-electron spectroscopy (XPS) was conducted using K-alpha (Thermo VG Scientific). Simultaneous thermogravimetric analysis-differential scanning calorimetry (TGA-DSC) plots were obtained by LABSYS Evo (SETARAM). Scanning electron microscopy and energy-dispersive X-ray spectroscopy (SEM-EDS) measurements were proceeded by JSM-IT800 (JEOL). The dried powder samples were loaded on carbon tapes to the SEM-EDS analysis.

S2. Crystal Structures of PdOF-1 and Their Structural Transformation

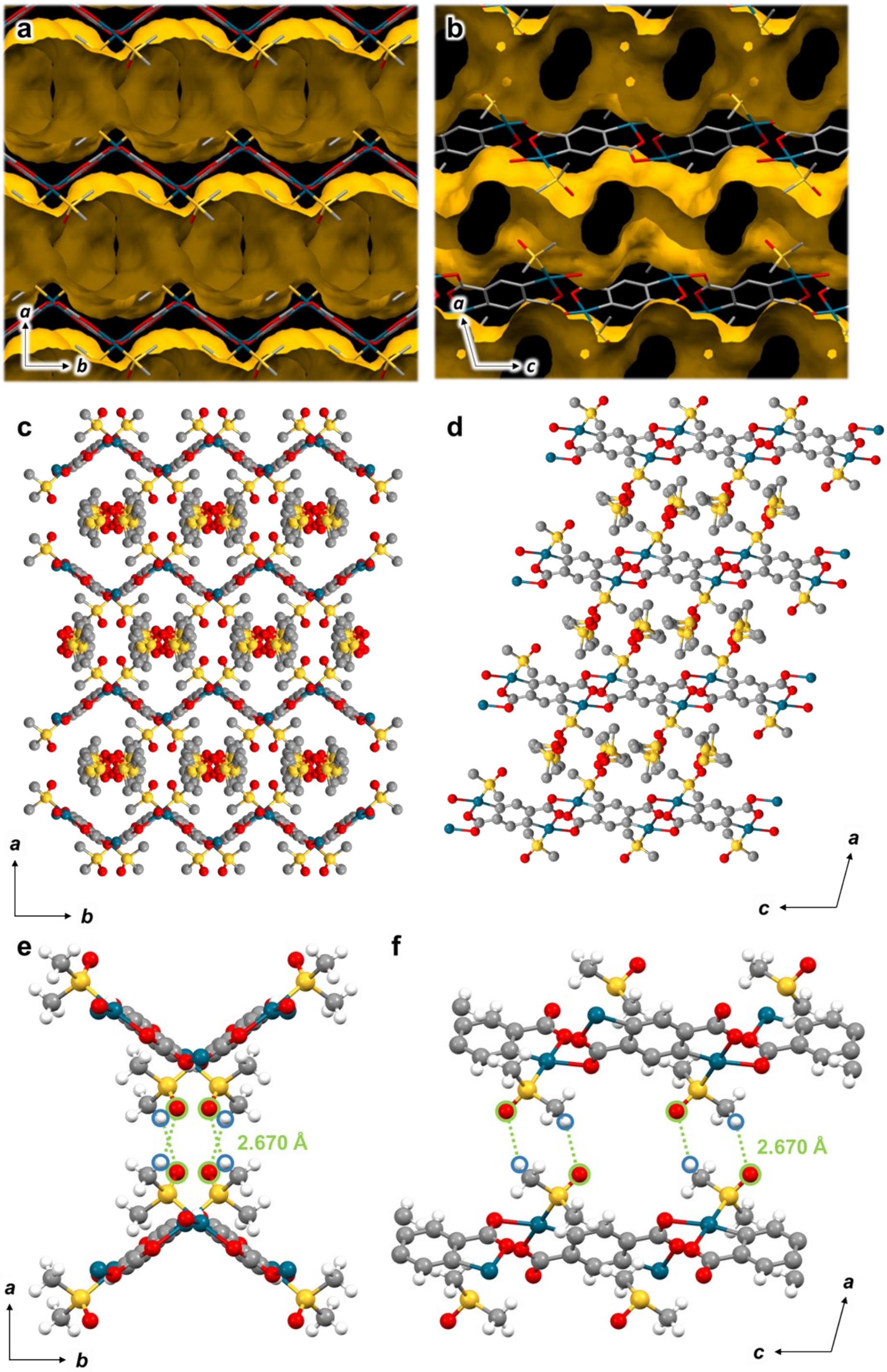

Figure S1. 2D intersecting channels in PdOF-1(A) (a) along the *c*-axis, and (b) along the *b*-axis, with yellow surface representing void spaces. Intercalating DMSO solvents and hydrogen atoms were excluded for clarity. Crystal structures of PdOF-1(A) with intercalated DMSO molecules along the (c) c-axis and (d) b-axis. Interlayer interactions in PdOF-1(A) between O atoms (green circles) and H atoms (blue circles) of DMSO molecules (e) along the *c*-axis, and (f) along the *b*-axis. The measured distance between two atoms is 2.670 Å.

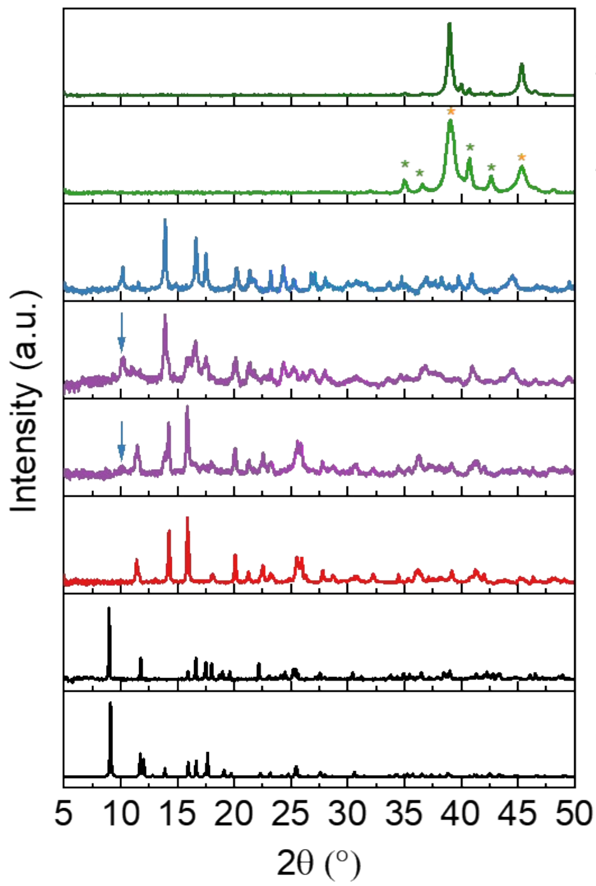

Figure S2. PXRD patterns of PdOF-1 after heating at various temperatures for 30 min. Blue arrows marked the appearance of PdOF-1(C) at 150 and 170 °C. Peaks marked with yellow and green stars indicate the formation of Pd and Pd_4S nanoparticles, respectively.

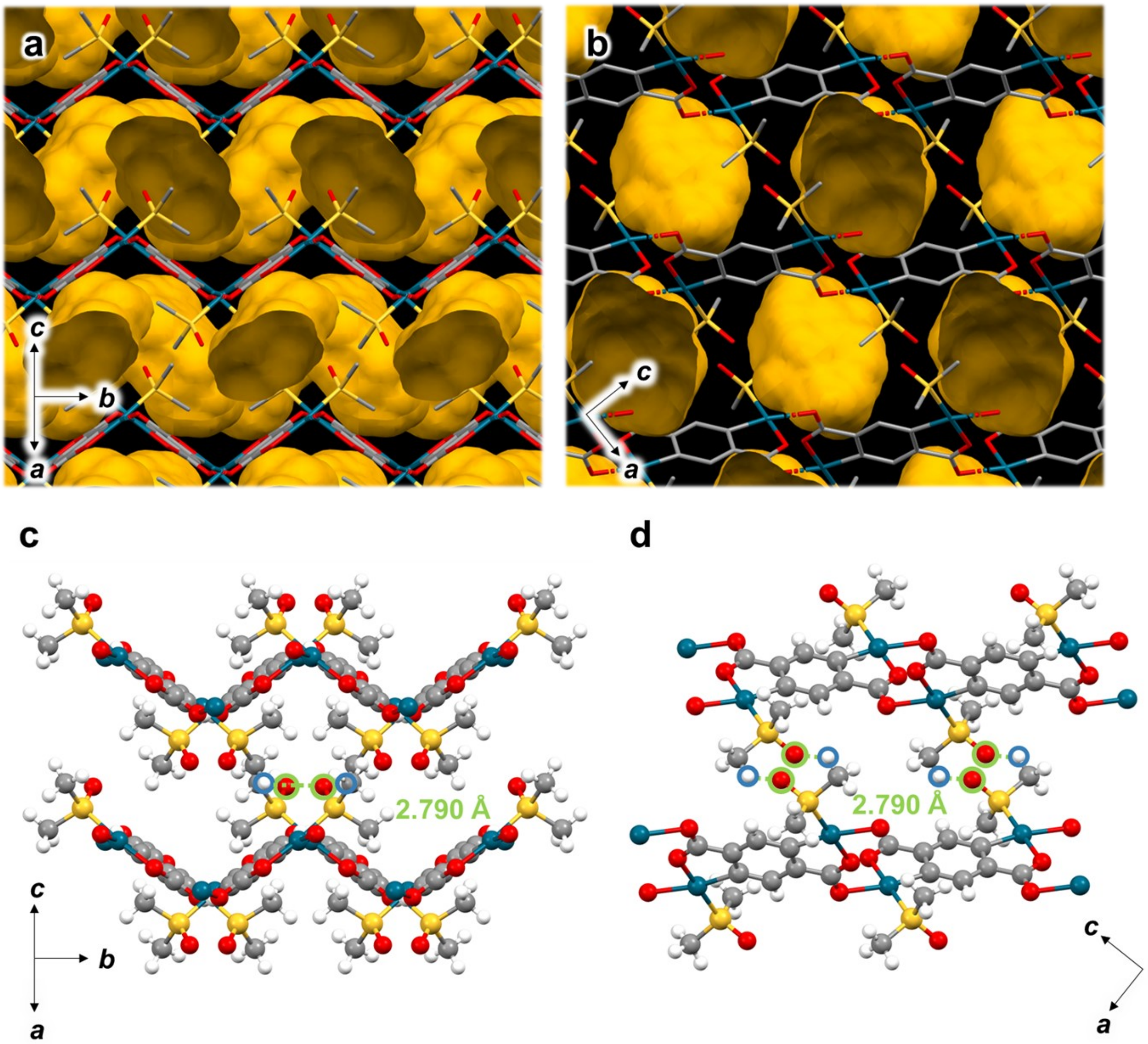

Figure S3. Disconnected void spaces in PdOF-1(B) (a) along the *ac*-plane, and (b) along the *b*-axis, with yellow surface representing void spaces. Intercalating DMSO solvents and hydrogen atoms were excluded for clarity. Interlayer interactions in PdOF-1(A) between O atoms (green circles) and H atoms (blue circles) of DMSO molecules (c) along the *ac*-plane, and (d) along the *b*-axis. The measured distance between two atoms is 2.790 Å.

Gas sorption measurements were conducted to evaluate the permanent porosity of PdOF-1(B). N_2 gas adsorption measurements were performed on PdOF-1(B) using a Micromeritics 3Flex instrument. Prior to analysis, the sample was degassed under vacuum at 100 °C for 12 h, a condition confirmed to avoid further transformation to PdOF-1(C). However, the resulting BET and Langmuir surface areas were determined to be 0.94 and 1.0 $m^2\ g^{-1}$, respectively, indicating minimal accessible porosity after solvent removal.

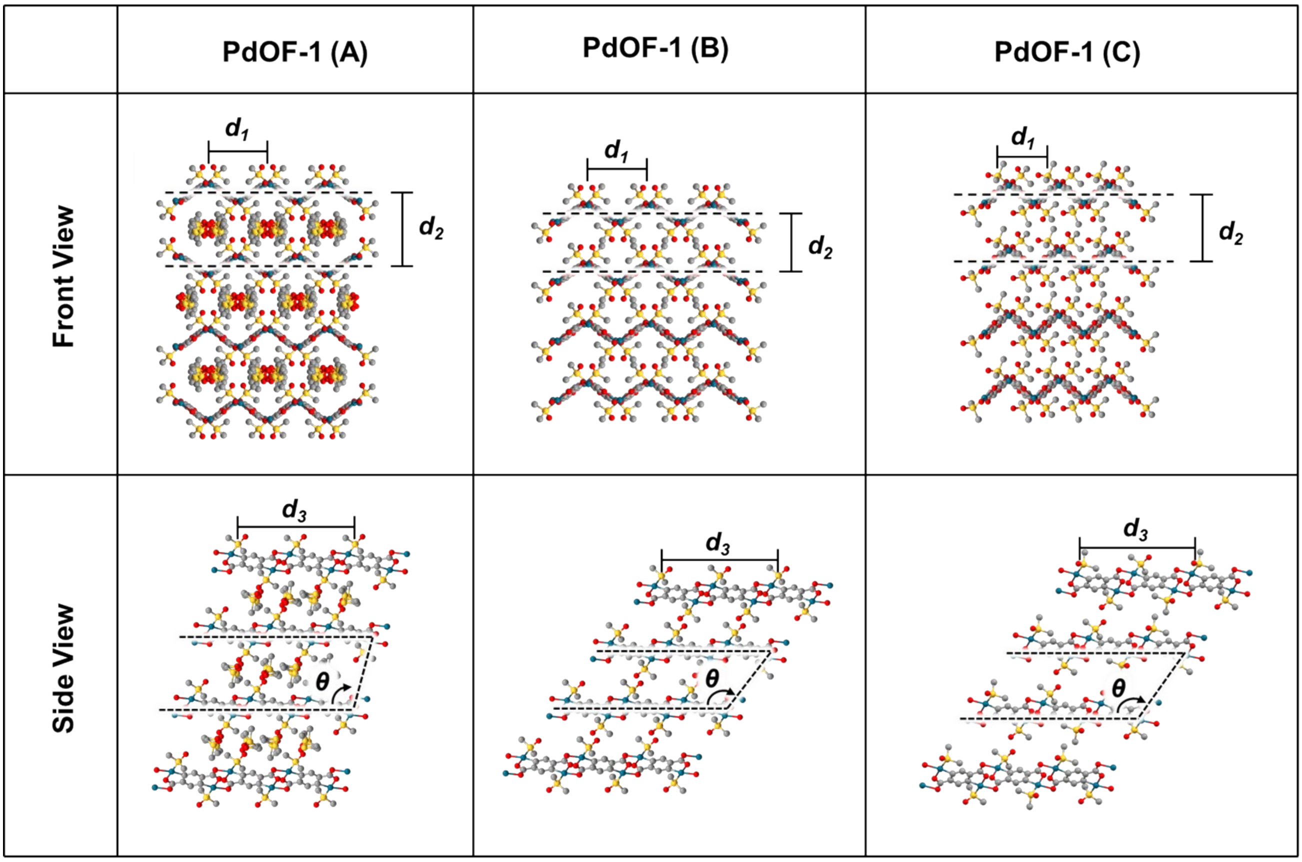

Figure S4. Crystal structures of PdOF-1(A), PdOF-1(B), and PdOF-1(C) with four distinct structural features: pitch (d_1), interlayer spacing (d_2), interval (d_3), and inclined stacking angle(θ). The calculated structural features are represented in **Table S1**.

Table S1. Calculated structural features of three PdOF-1 phases.

	PdOF-1(A)	PdOF-1(B)	PdOF-1(C)
Pitch (d_1)	7.9 Å	8.0 Å	6.7 Å
Interlayer spacing (d_2)	9.7 Å	7.6 Å	8.7 Å
Interval (d_3)	15.6 Å	15.6 Å	15.5 Å
Inclined stacking angle (θ)	105°	128°	125°
Torsional angle ($\Phi_{C–O–Pd–O}$)	104°	100°	83°
Porosity	42%	19%	12%

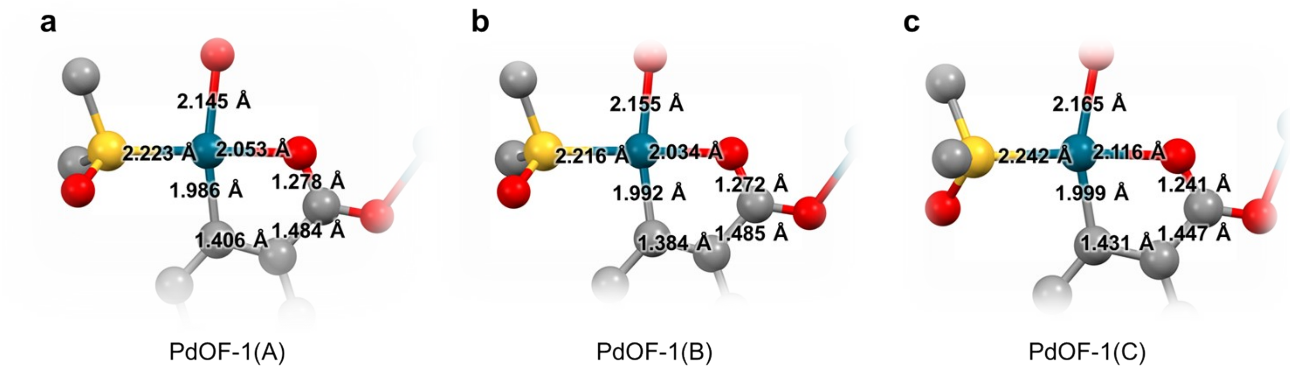

Figure S5. Local molecular environments of Pd atoms in (a) PdOF-1(A), (b) PdOF-1(B), and (c) PdOF-1(C). Inset numbers indicate interatomic distances. The Pd–C bond lengths progressively increased from 1.986 Å in PdOF-1(A) to 1.992 Å in PdOF-1(B) and 1.999 Å in PdOF-1(C), corresponding to the phase transformations. Interestingly, the Pd–O bond, which bridges two rigid units as shown in **Figure 1a**, gradually lengthened from 2.145 Å in PdOF-1(A) to 2.155 Å in PdOF-1(B) and 2.165 Å in PdOF-1(C).

S3. Spectral Characterization of PdOF-1(B) and PdOF-1(C)

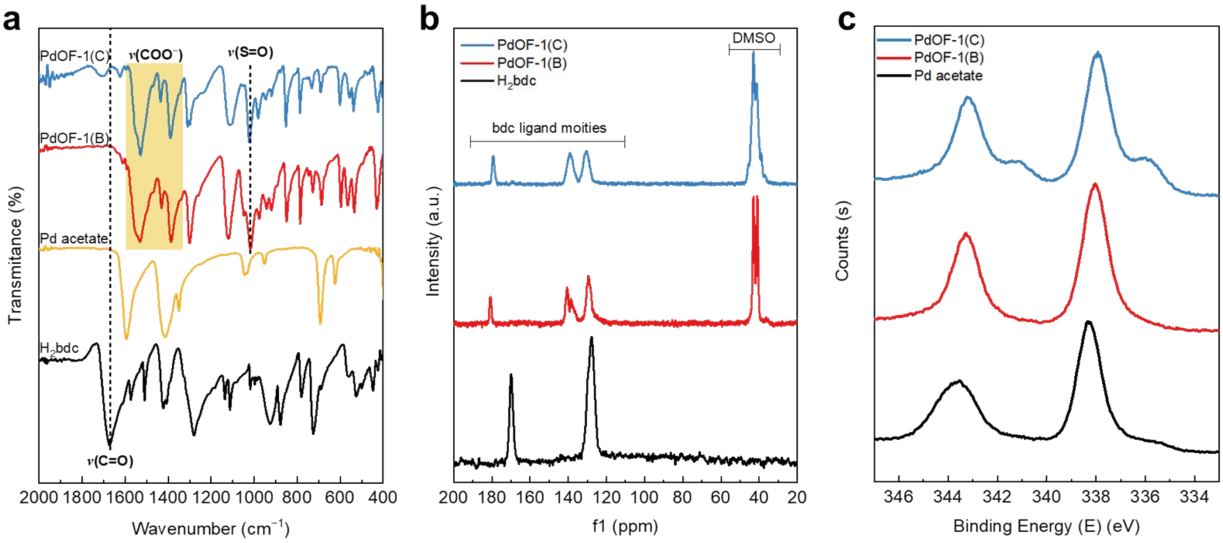

Figure S6. Spectroscopic analyses of the PdOF-1. (a) FT-IR, (b) ^{13}C CP-MAS NMR, and (c) XPS spectra of PdOF-1(B) and PdOF-1(C) with reactants.

For supporting the crystal structure of PdOF-1(B) and PdOF-1(C), spectral analyses FT-IR, ^{13}C CP-MAS NMR, and XPS were conducted. FT-IR spectroscopy confirmed the bonding within the framework (**Figure S6a**). The FT-IR spectra for both PdOF-1(B) and PdOF-1(C) phases revealed the symmetric and asymmetric carboxylate stretching modes of the bdc^{2-} ligand, without any C=O stretching mode associated with unbound H_2bdc ligands at $\tilde{\nu}$ = 1690 cm^{-1}, confirming successful bonding of bdc^{2-} ligands to Pd atoms. Stretching modes corresponding to S=O was discernible at $\tilde{\nu}$ = 1022 cm^{-1}. Importantly, the spectra of PdOF-1(B) and PdOF-1(C) were similar, suggesting that the topology of the 2D lattice remained.

^{13}C CP-MAS NMR further confirmed the bonding of bdc^{2-} ligands in both PdOF-1(B) and PdOF-1(C) phases (**Figure S6b**). For H_2bdc, the chemical shifts at 170 and 128 ppm corresponded to the C atoms of carboxylates and aromatic rings, respectively. The chemical shift at 170 ppm was absent after the reaction, indicating the bonding of the carboxylates. Instead, the strong deshielding effect of Pd on C atoms of carboxylates resulted in shifts to 181 and 179 ppm for PdOF-1(B) and PdOF-1(C), respectively. Additionally, Pd–C bonding on aromatic rings was indicated by new deshielded chemical shifts at 138-141 ppm appearing after reactions.

The Pd 3d spectra exhibit binding energies at 338.3, 338.0, and 337.9 eV for Pd acetate, PdOF-1(B), and PdOF-1(C), respectively, all of which are consistent with Pd(II) species and agree well with the structural information (**Figure S6c**). The slight shifts observed for PdOF-1(B) and PdOF-1(C) relative to Pd acetate reflect changes in the coordination environment of the Pd(II) centers within the framework. Notably, the nearly identical Pd 3d peak positions for PdOF-1(B) and PdOF-1(C) indicate that the square-planar coordination geometry of Pd(II) is largely preserved across these phases. In the case of PdOF-1(C), a minor shoulder at 335.8 eV was detected, which can be attributed to Pd(0) nanoparticles formed from over-reduction during thermal treatment. As the XPS signal represents an ensemble average of the surface of powders, this feature likely arises from a small fraction of surface Pd species.

S4. Molar Ratio Calculation from TGA Plots and Elemental Analysis

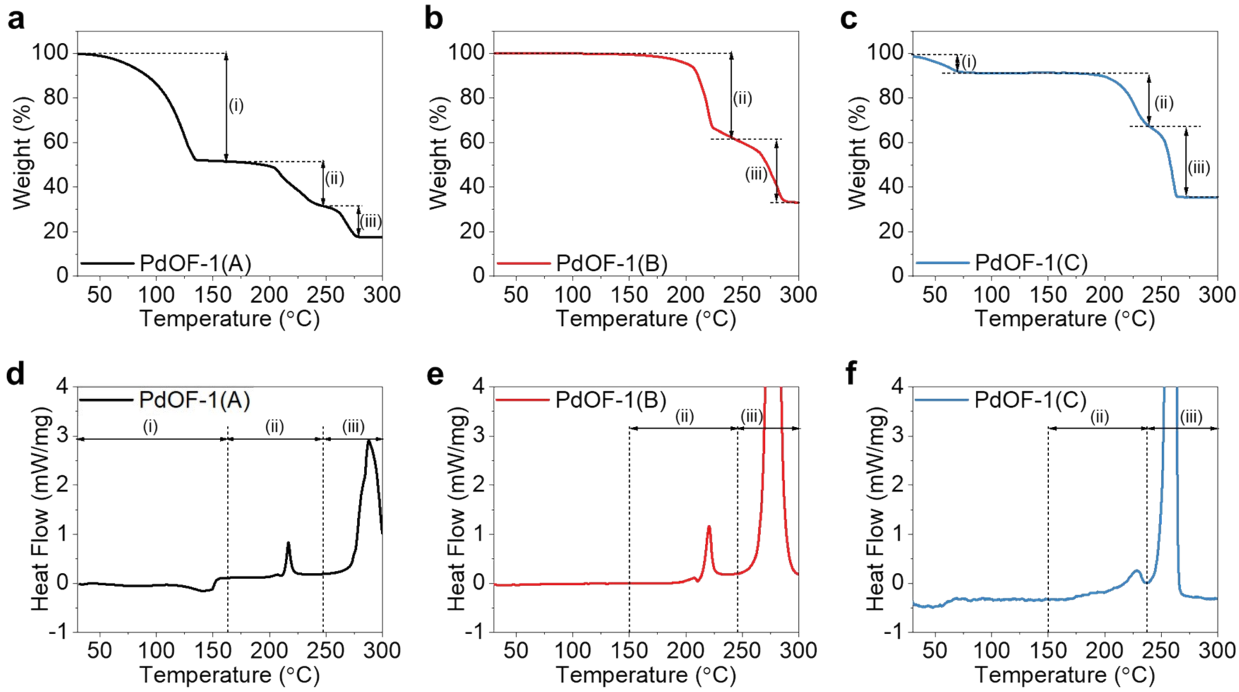

Figure S7. Thermal analysis of PdOF-1. TGA plots of (a) PdOF-1(A), (b) PdOF-1(B), and (c) PdOF-1(C). DSC plots of (d) PdOF-1(A), (e) PdOF-1(B), and (f) PdOF-1(C). The plots follow three distinct steps: (i) free solvents evaporation, (ii) DMSO decomposition, and (iii) bdc ligands degradation. The TGA and DSC measurements of PdOF-1 were conducted from room temperature to 300 °C at a heating rate of 2.5 °C/min under an air atmosphere.

Further investigation into the phase transformation of PdOF-1 was conducted using thermogravimetric analysis (TGA) and differential scanning calorimetry (DSC). The TGA and DSC plots of PdOF-1 revealed three distinct steps involving phase transformation. The first step, which stands out in the TGA and DSC plots of PdOF-1(A), occurred with a prolonged endothermic peak until the temperature reached to approximately 160 °C. The extreme mass loss of PdOF-1(A) during this step indicates evaporation of free DMSO solvents. The second step involving mass loss in all three phases began at 200 °C. In contrast to the endothermic peak of DMSO evaporation in the first step, the DSC plot in this region showed a sharp exothermic peak, indicating the thermal decomposition of DMSO rather than evaporation at high temperatures above the boiling point.[23,24] The final step occurred around 250 °C, marking the oxidative degradation of the bdc ligands and yielding residual metallic Pd(0) in all three phases.[25]

Table S2. Mass percentages of components in PdOF-1 across A, B, and C phases as evaluated by TGA.

	free solvent evaporation	DMSO decomposition	bdc degradation	residual Pd(0)
A phase	49.5%*	20.0%	13.8%	17.6%
B phase	-	38.7%	28.2%	33.1%
C phase	8.5%	24.5%	31.6%	35.4%

*Due to the significant amount of residual DMSO adhering to the surface of PdOF-1(A), the exact amount of evaporated DMSO from the intercalation in PdOF-1(A) could not be calculated.

Table S3. Mass ratio between components in PdOF-1 across A, B, and C phases as evaluated by TGA and SC-XRD. The theoretical values are based on the structure of PdOF-1 obtained from SC-XRD, assuming the absence of intercalated DMSO molecules. Under this assumption, the molecular formula of the unit is $Pd_2(bdc)(DMSO)_2$.

	DMSO*/bdc^{2-}	**DMSO*/Pd**	bdc^{2-}/Pd
Calculated ratio from the crystal structure of A phase: $Pd_2(bdc)(DMSO)_4$	1.84	**1.47**	0.771
A phase	-	**-**	0.784
B phase	1.37	**1.17**	0.852
C phase	0.775	**0.692**	0.893
Theoretical ratio without intercalated DMSO molecules: $Pd_2(bdc)(DMSO)_2$	0.952	**0.734**	0.771

*DMSO ratio was calculated based on the DMSO decomposition.

** Intercalated DMSO was excluded for calculating theoretical ratio.

Table S4. Molar ratio between components in PdOF-1 across A, B, and C phases as evaluated by TGA and SC-XRD. The theoretical values are based on the structure of PdOF-1 obtained from SC-XRD, assuming the absence of intercalated DMSO molecules. Under this assumption, the molecular formula of the unit is $Pd_2(bdc)(DMSO)_2$.

	DMSO*/bdc^{2-}	**DMSO*/Pd**	bdc^{2-}/Pd
Calculated ratio from the crystal structure of A phase: $Pd_2(bdc)(DMSO)_4$	4.00	**2.00**	0.500
A phase	-	**-**	0.508
B phase	2.88	**1.59**	0.553
C phase	1.63	**0.943**	0.579
Theoretical ratio without intercalated DMSO molecules: $Pd_2(bdc)(DMSO)_2$	2.00	**1.00**	0.500

*DMSO ratio is calculated based on DMSO decomposition.

** Intercalated DMSO is excluded for calculating theoretical ratio.

The distinguishable mass loss in the three PdOF-1 phases during the DMSO evaporation and DMSO decomposition indicates that each phase has different DMSO content. To quantify the DMSO content, the molar ratio of contents in PdOF-1 was examined by calculating the mass loss at each step from TGA plots and by elemental analysis (**Table S2-4**). Due to the significant residual DMSO adhering to the wet crystal surface, direct quantification of the DMSO content in PdOF-1(A) from the TGA plot was unreliable. Nonetheless, the DMSO-to-Pd ratio in PdOF-1(A) was reliably estimated from its crystal structure, yielding a S-to-Pd ratio of 2. After structural transformation via thermal treatments, the DMSO-to-Pd ratio of PdOF-1(B) and PdOF-1(C) were 1.59 and 0.943, respectively. These values obtained by TGA-DSC measurements closely match the scanning electron microscopy–energy dispersive X-ray spectroscopy (SEM-EDS) analyses, which showed DMSO-to-Pd ratios of 1.60 ± 0.14 in PdOF-1(B) and 0.89 ± 0.02 in PdOF-1(C). These results clearly show that the DMSO content gradually decreases as the phase transformation proceeds.

S5. Solvent Exchange

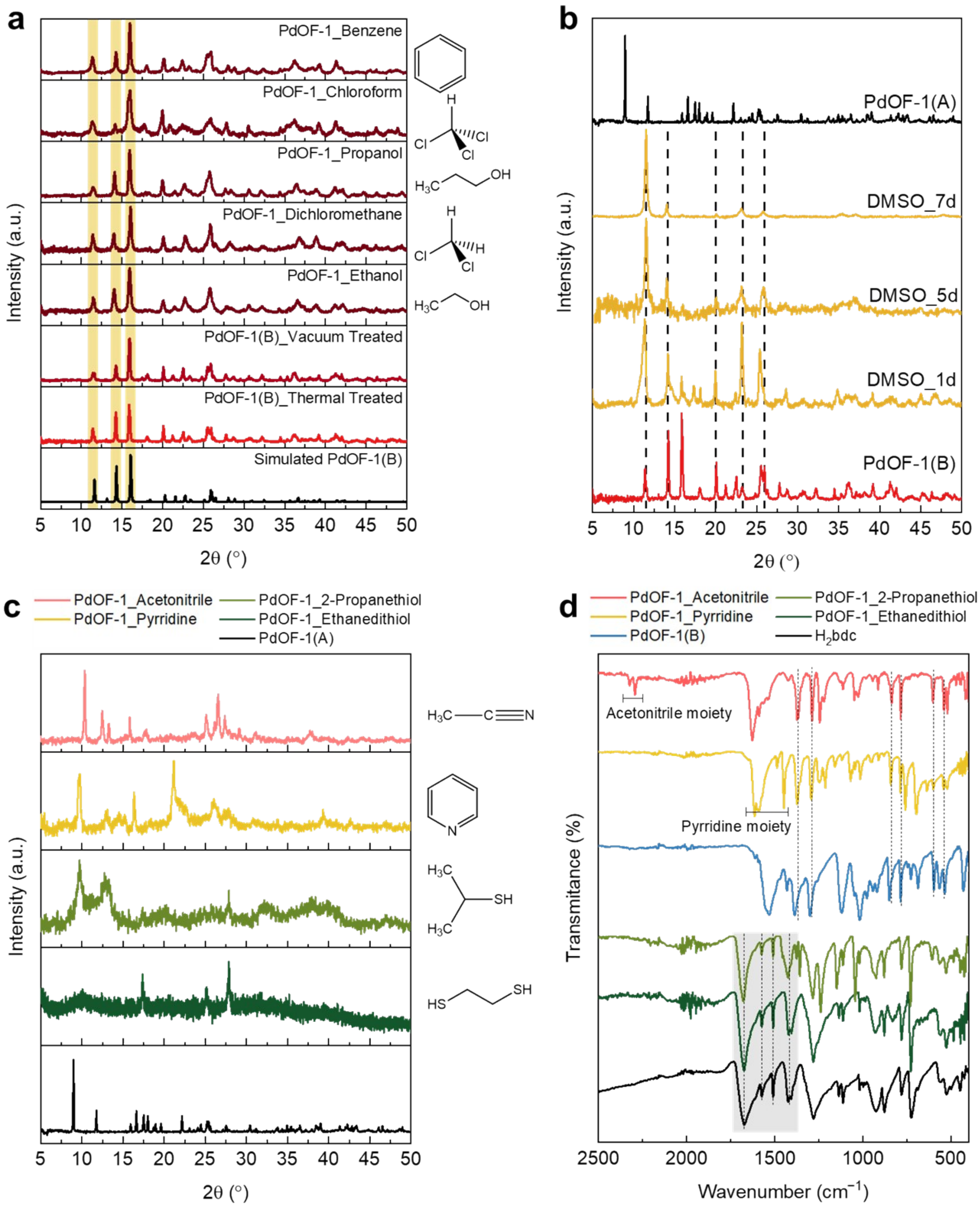

Figure S8. Solvent exchange treatments. (a) PXRD patterns of simulated PdOF-1(B) and experimental PdOF-1(B) obtained through thermal, vacuum drying, and solvent exchanges. Yellow boxes indicate three representative peaks at 2θ = 11.6˚, 14.3˚, and 16.0˚, corresponding to $(10\bar{1})$, (002), and $(11\bar{1})$ planes, respectively. (b) PXRD patterns of PdOF-1(A) (black), PdOF-1(B) (red), and immersed PdOF-1(B) in DMSO for 1, 5, and 7 days (yellow). (c) PXRD patterns of pristine PdOF-1(A) (black) and samples after solvent exchange. (d) FT-IR spectra of H_2bdc (black dashed), PdOF-1(B) (blue) and solvent exchanged samples. The gray box and black bottom dashed lines highlight characteristic peaks of H_2bdc. Upper dashed lines highlight characteristic peaks of PdOF-1(B) which also appears at the spectra of acetonitrile and pyridine exchanged samples.

To investigate the influence of solvents on the structural transformation of pristine PdOF–1(A), we monitored changes in the framework after solvent exchange treatments. Solvent exchanges using low-boiling-point organic solvents—including benzene, chloroform, 1-propanol, dichloromethane, and ethanol—converted PdOF-1(A) into PdOF-1(B) (**Figure S8a**). Similarly, vacuum drying also induced this transformation. These observations suggest that the reduction of intercalated DMSO molecules drive the A-to-B phase transition, which can thus be achieved via thermal drying, vacuum drying, or exchange with inert organic solvents.

In addition, to examine the reversibility of the structural transformation between PdOF-1(A) and PdOF-1(B), the temporal evolution of PdOF-1(B) immersed in DMSO was monitored by PXRD (**Figure S8b**). The reverse transformation from PdOF-1(B) to PdOF-1(A) was not observed, indicating the host-guest interaction between DMSO solvents and the frameworks are insufficient to overcome the energy barrier of restoring PdOF-1(A) phase. Notably, although the peak positions remained unchanged over a week, significant changes in peak intensities were observed. In particular, the reflection at $2\theta = 11.6°$, corresponding to the interlayer spacing, became markedly intensified, suggesting re-ordering of the layered structure induced by prolonged exposure to DMSO, rather than phase reversion.

In contrast, solvent exchange using coordinating solvents such as acetonitrile, pyridine, 2-propanethiol, and ethanedithiol resulted in distinct PXRD patterns (**Figure S8c**). In particular, thiol-containing solvents, 2-propanethiol and ethanedithiol, reacted with PdOF-1(A), leading to structural disassembly. FT-IR spectra of the resulting solids exhibited characteristic peaks corresponding to free H_2bdc, indicating degradation of the Pd-based networks (**Figure S8d**).

Interestingly, acetonitrile and pyridine—known to coordinate with Pd atoms through Pd–N bonds—converted PdOF-1(A) into new crystalline phases. In both cases, PXRD patterns confirmed the retention of crystallinity, and FT-IR spectra showed no evidence of liberated H_2bdc ligands (**Figure S8c**). Notably, the lowest-angle diffraction peaks, corresponding to the interlayer spacing in our frameworks, shifted from $2\theta = 9.1°$ (9.7 Å) in PdOF-1(A) to 10.4° (8.5 Å) and 9.7° (9.1 Å) after exchange with acetonitrile and pyridine, respectively. Although the crystallinity of these resulted phases was insufficient for full structure determination via SC-XRD, these solvent-induced phase transformations highlight the organometallic nature of PdOF-1 and its potential for organometallic applications. Furthermore, FT-IR spectra of the exchanged samples revealed vibrational bands corresponding to coordinated acetonitrile and pyridine, confirming their interaction with the Pd centers (**Figure S8d**).[26,27]

S6. Supporting References

1 *SHELXTL Software Reference Manual*, Bruker AXS Inc., 5465 East Cheryl Parkway, Madison, WI 53711., 1997.

2 G. M. Sheldrick, *Acta Crystallogr. A*, 2008, **64**, 112–122.

3 G. M. Sheldrick, *Acta Crystallogr. A*, 1990, **46**, 467–473.

4 G. M. Sheldrick, *Acta Crystallogr. A*, 2015, **71**, 3–8.

5 G. M. Sheldrick, *Acta Crystallogr. C Struct. Chem.*, 2015, **71**, 3–8.

6 J. W. Shin, K. Eom and D. Moon, *J. Synchrotron Radiat.*, 2016, **23**, 369–373.

7 Z. Otwinowski and W. Minor, *Methods Enzymol.*, 1997, **276**, 307–326.

8 O. V. Dolomanov, L. J. Bourhis, R. J. Gildea, J. A. K. Howard and H. Puschmann, *J. Appl. Crystallogr.*, 2009, **42**, 339–341.

9 L. J. Bourhis, O. V. Dolomanov, R. J. Gildea, J. A. K. Howard and H. Puschmann, *Acta Crystallogr. A Found. Adv.*, 2015, **71**, 59–75.

10 P. van der Sluis and A. L. Spek, *Acta Crystallogr. A*, 1990, **46**, 194–201.

11 S. Kwon, H. S. Shin, J. Gong, J.-H. Eom, A. Jeon, S. H. Yoo, I. S. Chung, S. J. Cho and H.-S. Lee, *J. Am. Chem. Soc.*, 2011, **133**, 17618–17621.

12 R. Shirley, *The CRYSFIRE system for automatic powder indexing: user's manual*, Lattice Press, Guildford UK, 2000.

13 R. Černý and V. Favre-Nicolin, *Z. Kristallogr. Cryst. Mater.*, 2007, **222**, 105–113.

14 V. Favre-Nicolin and R. Černý, *J. Appl. Crystallogr.*, 2002, **35**, 734–743.

15 V. Favre-Nicolin and R. Černý, *Z. Kristallogr. Cryst. Mater.*, 2004, **219**, 847–856.

16 A. C. Larson and R. B. Von Dreele, *General Structure Analysis System (GSAS)*, Los Alamos National Laboratory Report LAUR 86-748, 2004.

17 B. H. Toby, *J. Appl. Crystallogr.*, 2001, **34**, 210–213.

18 P. Thompson, D. E. Cox and J. B. Hastings, *J. Appl. Crystallogr.*, 1987, **20**, 79–83.

19 L. W. Finger, D. E. Cox and A. P. Jephcoat, *J. Appl. Crystallogr.*, 1994, **27**, 892–900.

20 P. W. Stephens, *J. Appl. Crystallogr.*, 1999, **32**, 281–289.

21 C. F. Macrae, I. Sovago, S. J. Cottrell, P. T. A. Galek, P. McCabe, E. Pidcock, M. Platings, G. P. Shields, J. S. Stevens, M. Towler and P. A. Wood, *J. Appl. Crystallogr.*, 2020, **53**, 226–235.

22 L. J. Barbour, *Chem. Commun.*, 2006, 1163–1168.

23 B. T. Brandes and D. K. Smith, *Process Saf. Prog.*, 2016, **35**, 374–391.

24 Q. Yang, M. Sheng, X. Li, C. Tucker, S. Vásquez Céspedes, N. J. Webb, G. T. Whiteker and J. Yu, *Org. Process Res. Dev.*, 2020, **24**, 916–939.

25 J. Pires, *J. Inorg. Organomet. Polym. Mater.*, 2024, **34**, 3346–3359.

26 B. Dereka, N. H. C. Lewis, J. H. Keim, S. A. Snyder and A. Tokmakoff, *J. Phys. Chem. B*, 2022, **126**, 278–291.

27 M. I. Zaki, M. A. Hasan, F. A. Al-Sagheer and L. Pasupulety, *Colloids Surf. A Physicochem. Eng. Asp.*, 2001, **190**, 261–274.

Appendix

Crystallographic Data of PdOF-1(A), PdOF-1(B), and PdOF-1(C)

Crystallographic data of PdOF-1(A) (CCDC 2481799)

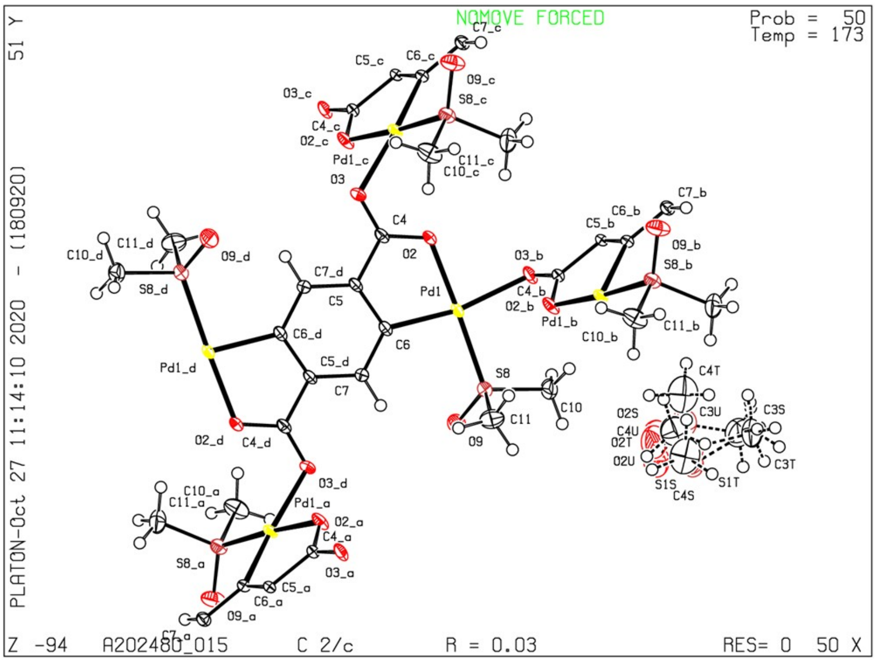

Figure S9. ORTEP for PdOF-1(A). Ellipsoids are depicted at 50% probability.

Table S5. Crystal data and structure refinement for PdOF-1(A)

Empirical formula	$C_8 H_{13} O_4 Pd S_2$	
Formula weight	343.70	
Temperature	173(2) K	
Wavelength	0.71073 Å	
Crystal system	Monoclinic	
Space group	*C*2/*c*	
Unit cell dimensions	a = 20.1486(8) Å	α = 90°
	b = 7.9481(3) Å	β = 105.2716(13)°
	c = 15.6495(6) Å	γ = 90°
Volume	2417.66(16) Å^3	
Z	8	
Density (calculated)	1.889 Mg/m^3	
Absorption coefficient	1.871 mm^{-1}	
F(000)	1368	
Crystal size	0.134 x 0.062 x 0.042 mm^3	
Theta range for data collection	3.199 to 27.497°.	
Index ranges	–26<=h<=24, –10<=k<=10, –20<=l<=20	
Reflections collected	23417	
Independent reflections	2761 [R(int) = 0.0365]	
Completeness to theta = 25.242°	99.5 %	
Absorption correction	Semi-empirical from equivalents	
Max. and min. transmission	0.7456 and 0.6256	
Refinement method	Full-matrix least-squares on F^2	
Data / restraints / parameters	2761 / 313 / 219	
Goodness-of-fit on F^2	1.137	
Final R indices [I>2sigma(I)]	R1 = 0.0284, wR2 = 0.0525	
R indices (all data)	R1 = 0.0339, wR2 = 0.0544	
Largest diff. peak and hole	0.485 and –0.895 e·Å^{-3}	

Crystallographic data of PdOF-1(B) (CCDC 2189180)

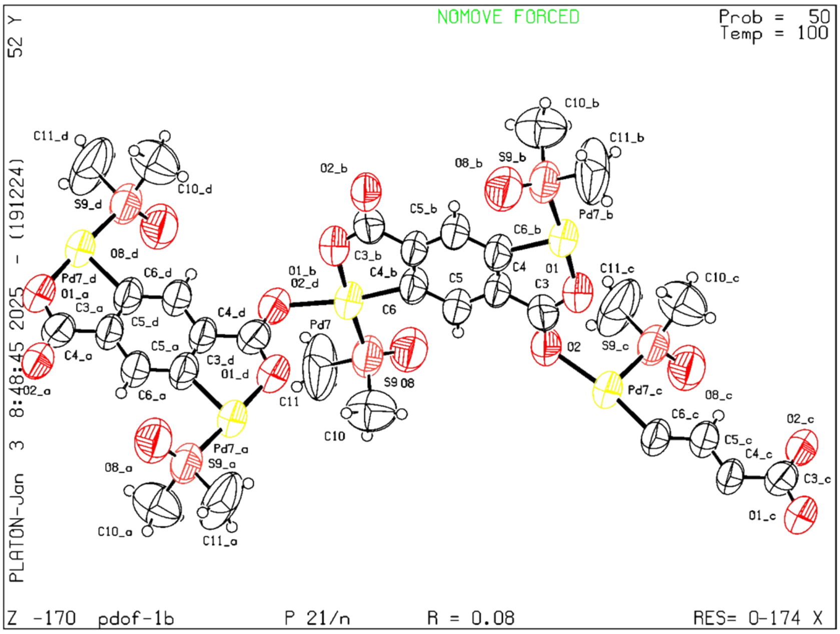

Figure S10. ORTEP for PdOF-1(B). Ellipsoids are depicted at 50% probability.

Table S6. Crystal data and structure refinement for PdOF-1(B)

Empirical formula	$C_7 H_{10} O_3 Pd S_{1.5}$	
Formula weight	304.64	
Temperature	100 K	
Wavelength	0.700 Å	
Crystal system	Monoclinic	
Space group	$P2_1/n$	
Unit cell dimensions	a = 9.6020(19) Å	α = 90°
	b = 8.0050(16) Å	β = 90.43(3)°
	c = 12.364(3) Å	γ = 90°
Volume	950.3(3) Å^3	
Z	4	
Density (calculated)	2.129 Mg/m^3	
Absorption coefficient	2.172 mm^{-1}	
F(000)	600.0	
Crystal size	0.04 x 0.04 x 0.01 mm^3	
Theta range for data collection	2.636 to 24.999°.	
Index ranges	–11<=h<=11, –9<=k<=9, –14<=l<=14	
Reflections collected	5675	
Independent reflections	1737 [R(int) = 0.0904]	
Completeness to theta = 25°	99.5 %	
Absorption correction	Empirical	
Max. and min. transmission	1.000 and 0.758	
Refinement method	Full-matrix least-squares on F^2	
Data / restraints / parameters	1737 / 5 / 102	
Goodness-of-fit on F^2	0.829	
Final R indices [I>2sigma(I)]	R1 = 0.0794, wR2 = 0.2024	
R indices (all data)	R1 = 0.1439, wR2 = 0.2396	
Largest diff. peak and hole	1.01 and –1.18 e·Å^{-3}	

Crystallographic data of PdOF-1(C)

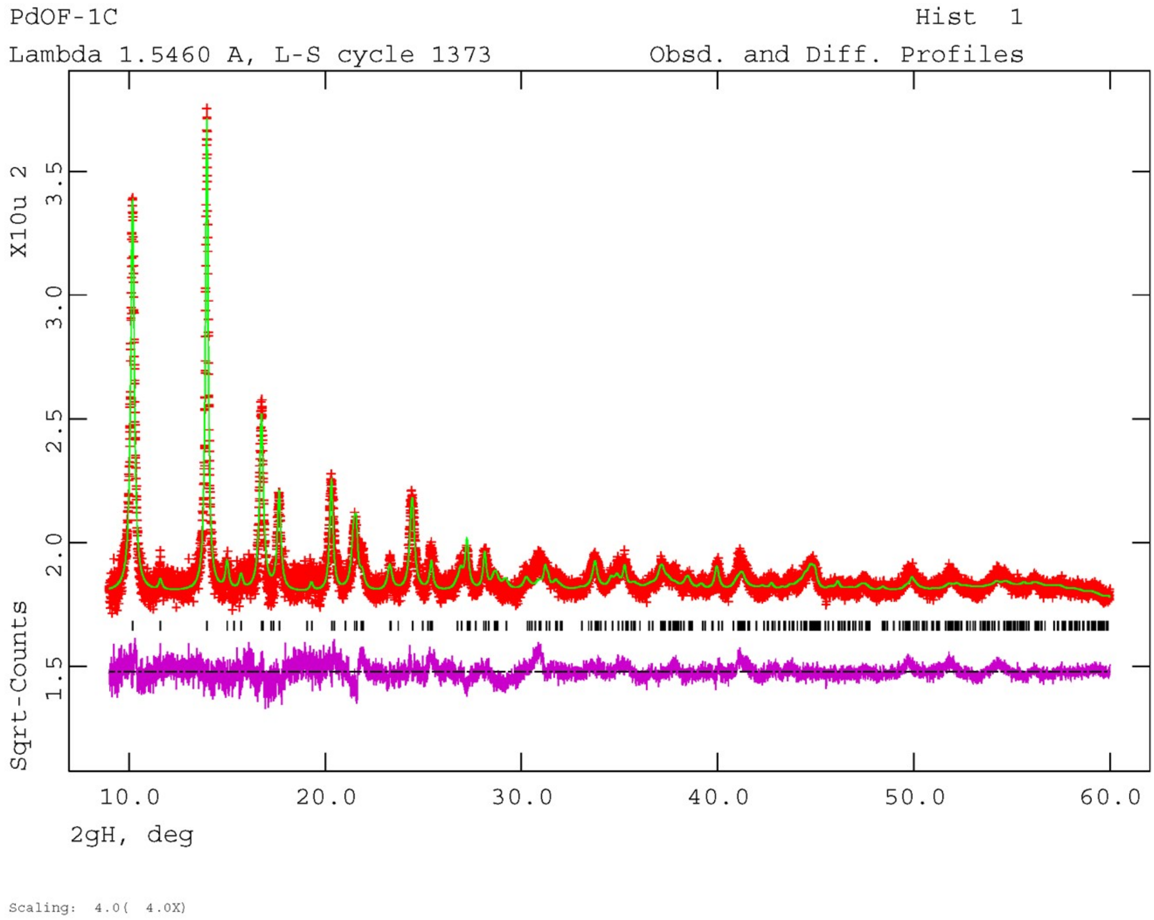

Figure S11. Final Rietveld plot of PdOF-1(C). Observed data points are denoted in red crosses, the simulated pattern (upper trace) and the difference pattern (lower trace) in green and pink solid lines, respectively.

Table S7. Crystal data and structure refinement for PdOF-1(C)

Crystal data	**PdOF-1(C)**
Chemical formula*	C_6O_3PdS
M_r*	258.82
Z	4
Z'	2
Symmetry	Monoclinic
Space group	$P2_1$
a, Å	15.5437 (21)
b, Å	6.6832 (6)
c, Å	10.6533 (16)
α, °	90
β, °	125.223 (9)
γ, °	90
Cell volume, Å^3	904.07 (19)
Specimen form, color	Powder, dark brown
Specimen preparation temperature	Room temperature
Data collection	
Diffractometer	9B High-resolution powder diffraction bemaline at Pohang Accelerator Laboratory
Data collection method	Specimen mounting: flat-plate polycarbonate holder, Mode: Bragg-Brentano geometry, Step scan method
Temperature, K	298
Radiation wavelength, Å	1.54600

2θ range, ° (range in Refinement)	8.5 – 60
Step size, °	0.005

Refinement	
Refinement on	Intensities
Least-squares matrix	Full-matrix
Goodness of fit	1.74
R factors	R_p = 0.0247, R_{wp} = 0.0329, R_{exp} = 0.0214, $R(F^2)$ = 0.20206
Excluded region(s)	None
Radiation polarization ratio	0.99
Profile function	CW Profile function number 4 with 21 terms #1(GU) = 0.000, #2(GV) = 0.000, #3(GW) = 0.000, #4(GP) = 0.000, #5(LX) = 9.615, #6(ptec) = 0.00, #7(trns) = 20.79, #8(shft) = -5.8634, #9(sfec) = 0.00, #10(S/L) = 0.0100, #11(H/L) = 0.0100, #12(eta) = 1.0000, #13(S400) = 0.04727, #14(S040) = 5.098, #15(S004) = 1.627, #16(S220) = 0.000, #17(S202) = 0.000, #18(S022) = 0.000, #19(S301) = 0.000, #20(S103) = 0.000, #21(S121) = 0.000. Peak tails are ignored where the intensity is below 0.0010 times the peak. Anisotropic broadening axis 0.0 0.0 1.0.
No. parameters	86
No. restraints	88
No. data points	10201
H-atom treatment*	Omitted during the refinement process
Background function	GSAS Background function number 1 with 8 terms, Shifted Chebyshev function of 1st kind. 1: 2028.05, 2: -3.54243, 3: -13.8062, 4: -14.7322, 5: -12.0742, 6: -18.9947, 7: -20.0532, 8: -7.44453
$(\Delta/\sigma)_{max}$, $(\Delta/\sigma)_{mean}$	0.03, 0.00

*H-atoms were omitted during the structure determination process.

Table S8. Atomic coordinates, thermal displacement parameter and occupancy for PdOF-1(C)

Atom	x	y	z	Occupancy	Uiso (Å2)	Multiplicity
Pd1	0.02078(9)	-0.0941(7)	0.86300(13)	1	0.0970(13)	2
O2	0.03003(7)	0.11207(9)	1.01106(13)	1	0.0970(13)	2
O3	0.13023(12)	0.33204(14)	1.18856(31)	1	0.0970(13)	2
C4	0.11111(13)	0.21909(18)	1.08646(32)	1	0.0970(13)	2
C5	0.18080(15)	0.19359(18)	1.0378(4)	1	0.0970(13)	2
C6	0.15795(13)	0.03050(17)	0.93762(30)	1	0.0970(13)	2
C7	0.22492(21)	-0.00291(18)	0.8946(4)	1	0.0970(13)	2
S8	0.02345(15)	-0.33054(16)	0.71772(25)	1	0.0970(13)	2
O9	0.0528(4)	-0.26807(19)	0.6148(4)	1	0.0970(13)	2
C10	0.10848(33)	-0.52326(19)	0.8422(7)	1	0.0970(13)	2
C11	-0.10174(29)	-0.44487(19)	0.6124(8)	1	0.0970(13)	2
O12	0.46296(7)	0.19926(12)	0.97578(13)	1	0.0970(13)	2
O13	0.37035(12)	-0.03946(15)	0.81186(29)	1	0.0970(13)	2
C14	0.38655(13)	0.07970(18)	0.9093(4)	1	0.0970(13)	2
C15	0.31465(15)	0.10874(18)	0.9533(4)	1	0.0970(13)	2
C16	0.33632(13)	0.27408(18)	1.05141(31)	1	0.0970(13)	2
C17	0.26763(22)	0.31099(18)	1.0905(4)	1	0.0970(13)	2
Pd18	0.47365(9)	0.39789(13)	1.12789(13)	1	0.0970(13)	2
S19	0.47253(16)	0.62837(17)	1.27894(26)	1	0.0970(13)	2
O20	0.52095(28)	0.82224(19)	1.2906(5)	1	0.0970(13)	2

C21	0.34002(34)	0.66229(19)	1.2154(8)	1	0.0970(13)	2
C22	0.5332(5)	0.51917(19)	1.4630(5)	1	0.0970(13)	2